Evaluation of Various Types of Wall Boundary Conditions for the Boltzmann Equation

Christopher D. Wilson[1], Ramesh K. Agarwal[*2]

Boeing Company, St. Louis, MO 63166, USA; Washington University in St. Louis, Missouri 63130, USA

[1]christopher.d.wilson.pe@gmail.com; [*2]rka@wustl.edu

Abstract

This paper presents the evaluation of several solid wall boundary conditions when used in the numerical solution of the Boltzmann equation using the finite-difference/finite-volume methods. Five solid wall boundary conditions are considered: (a) adsorption, (b) specular reflection, (c) diffuse reflection, (d) Maxwellian reflection, and (e) adsorptive Maxwellian reflection. The boundary conditions are applied on a two-dimensional discretized velocity space mesh. Methods for applying the same boundary conditions on a three-dimensional velocity space grid are also presented. The boundary conditions are implemented for the numerical solution of the hypersonic rarefied flow over a flat plate using a three-dimensional generalized Boltzmann equation (GBE) solver. The derivatives that contribute to heat transfer and skin friction at the solid boundary are calculated and compared. Recommendations for further evaluation of the boundary conditions are made.

Keywords

Boltzmann Equation; Non-equilibrium Hypersonic Flows; Wall Boundary Conditions for Boltzmann Equation

Nomenclature

ξ_I = incident molecular velocity

ξ_r = reflected molecular velocity

F = probability density

n = unit normal vector

$A_{m,n}$ = cell area corresponding to node (m, n)

K = Boltzmann constant

m = molecular mass

T = characteristic temperature

c_f = skin friction coefficient

q = heat transfer

U = bulk velocity

M = Mach number

Introduction

Application of appropriate boundary conditions in the computational domain is crucial to obtaining accurate solutions for any problem to be solved analytically or numerically. Appropriate types of boundary conditions must be implemented on various boundaries of the computational domain. The various types of boundary conditions, and where they are applied in the computational domain, are discussed in the following sections. The main emphasis is placed on the solid wall boundary conditions for the solution of the Wang-Chang Uhlenbeck equation (Tcheremissine, 2002) or the Generalized Boltzmann Equation (GBE) (Agarwal and Tcheremissine, 2010; Wilson, Agarwal and Tcheremissine, 2011; Qian, Agarwal and Wilson, 2013; Qian, Agarwal and Wang, 2013). Five types of boundary conditions: (a) adsorptive, (b) specular reflection, (c) diffuse reflection, (d) Maxwellian reflection, and (e) adsorptive Maxwellian reflection are considered, implemented and evaluated for their accuracy in computing the skin friction and heat transfer on the solid wall.

Inflow, Symmetry, and Outflow Boundary Conditions

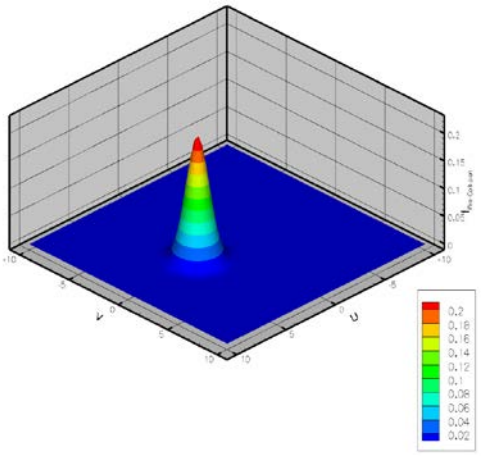

FIG. 1 MAXWELLIAN DISTRIBUTION AT THE INFLOW BOUNDARY, M = 3

The inflow boundary condition is assumed to be a Dirichlet boundary condition. Since the Boltzmann equation is a hyperbolic (wave-type) equation with the velocity distribution function as the dependent variable, the application of a Dirichlet boundary condition at the inflow boundary is accomplished by setting the inflow

value of the velocity distribution function. It is assumed that the inflow boundary is at equilibrium. Therefore, a Maxwellian distribution function centered at the mean velocity of the incoming flow is used at all the grid points at the inflow boundary. This condition is maintained at each time step. An example of the inflow boundary condition using the Maxwellian distribution function is shown in Figure 1.

A Neumann boundary condition is applied for all planes of symmetry by setting the partial derivative of the velocity distribution function with respect to the direction normal to the plane of symmetry equal to zero. The symmetry boundary conditions are implemented by imposing the condition that the velocity distribution function at (*i, j, k*) is equal to the distribution function at (*i-1, j-1, k-1*). This is a simple approach to ensure that the derivative is zero at the plane of symmetry. One note of caution is that the grid spacing near the plane of symmetry needs to be relatively small to ensure that the boundary condition does not adversely affect the calculations in the interior of the domain.

Solid Wall Boundary Conditions

Five solid wall boundary conditions are considered for application to the problem of flow around immersed bodies– adsorption, specular reflection, diffuse reflection, Maxwellian reflection, and adsorptive Maxwellian reflection. These boundary conditions range from relatively simple to be implemented to difficult, and from physically unrealistic to requiring tuning to match the empirical data. The formulation of each of these boundary conditions and their implementation are discussed in the following sections.

Adsorption Boundary Condition

An adsorptive boundary condition is the simplest of the solid wall boundary conditions to be implemented. The adsorptive boundary condition assumes that the molecular velocity reaches zero upon the wall. This concept is similar to the no-slip condition for viscous walls used in continuum flow solvers. However, for rarefied gases adsorption, it is implied that molecules continue to accumulate on the surface. Therefore, an adsorptive boundary condition needs to include a de-adsorptive phase so that the conservation laws are not violated at the boundary surface. Therefore, complete adsorption is physically unrealistic for a solid wall boundary and would result in a continuously increasing density at the boundary. Yet, the adsorptive boundary condition yields reasonable results for several macroscopic flow variables. However, as for the resolving of heat transfer and skin friction values at the solid boundary, a completely adsorptive boundary condition is not quite accurate. Therefore, other options for the solid wall boundary condition need to be considered.

There are two methods to implement an adsorptive boundary condition. One includes assigning all non-zero velocities a probability identical to zero. The total probability density of the incoming flow is then located entirely at the origin in velocity space. A finite value for probability density can be applied at the origin of velocity space, since the velocity space domain is finite-differenced. Obviously, as the finite volume decreases, the magnitude of the probability at the origin will increase toward infinity. An artificial adsorptive phase is implicitly applied by using this implementation. As a result, the probability density near the wall remains finite and does not increase exponentially over time. An alternative method is to take the probability densities of the upstream nodes and apply a corresponding Maxwellian distribution centered at zero velocity. This approach more directly addresses de-adsorption by providing finite probabilities that can be communicated upstream into the physical space domain. This approach to the adsorptive boundary condition, as applied in a two-dimensional velocity space, is illustrated in Figure 2.

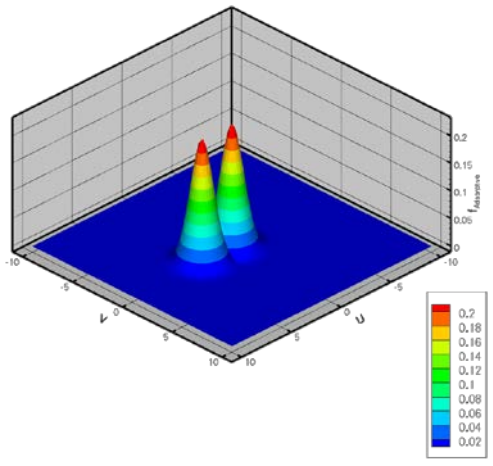

FIG. 2 ADSORPTIVE BOUNDARY CONDITION

At each time step, one of these two methods is applied to the distribution function at the boundary. It is important to note that the physical space finite-difference grid near the wall needs to be small in order to avoid introducing errors or instabilities during each iteration.

Specular Reflection Boundary Condition

The specular reflection boundary condition implies

that molecules reflect off of the solid wall similar to how light reflects off of a mirror (Figure 3). A fundamental assumption behind specular reflection is a completely smooth surface. Making that assumption is not completely realistic when molecular interactions are simulated with a surface.

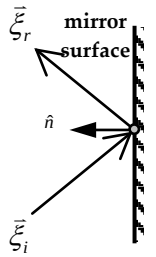

FIG. 3 SPECULAR REFLECTION

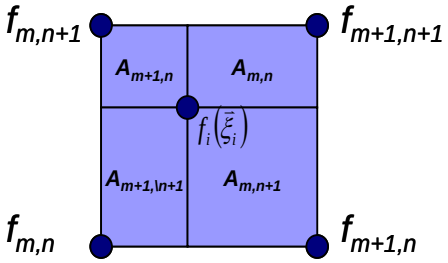

FIG. 4 VELOCITY SPACE GRID CELL INTERPOLATION

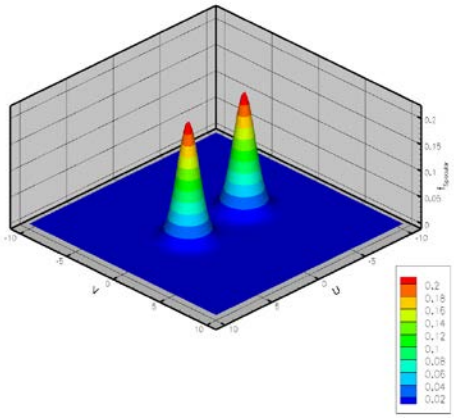

FIG. 5 SPECULAR REFLECTION BOUNDARY CONDITION, INCIDENT ANGLE = 90°

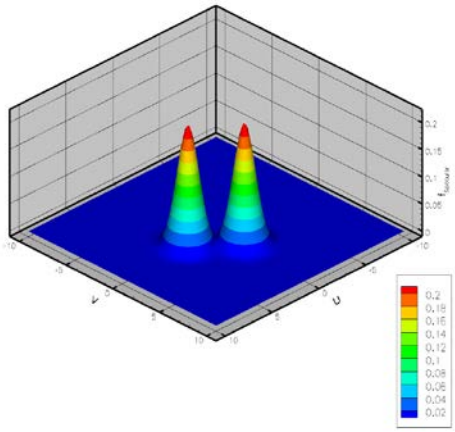

FIG. 6 SPECULAR REFLECTION BOUNDARY CONDITION, INCIDENT ANGLE = 45°

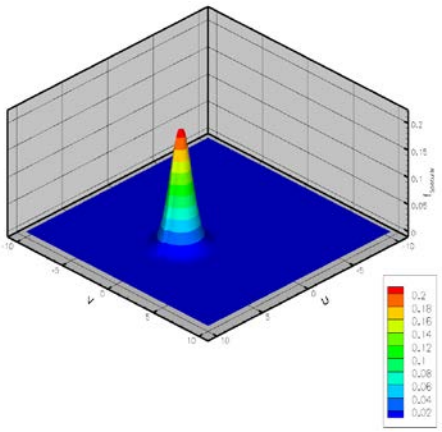

FIG. 7 SPECULAR REFLECTION BOUNDARY CONDITION, INCIDENT ANGLE = 0°

Implementing this boundary condition requires more bookkeeping than the adsorptive boundary condition. The magnitude of the velocity after the collision is the same as the velocity before the collision. However, the component of the velocity vector normal to the surface changes sign. The normal vector of the solid wall needs to be calculated at each physical space node. Then the reflected velocity can be related to the incident velocity using Equation 1. The velocity space grid points are assumed to be the velocity vectors for the reflected molecules. The probability for each point in the reflected velocity space is calculated using weighted area interpolation for a two-dimensional velocity space. Alternatively, a volume based interpolation can be used for a three-dimensional velocity space. The equation for a two-dimensional velocity space is given in Equation 2. The relationship between each of the neighbouring velocity space grid points and the point inside the velocity space grid cell is shown in Figure 4. The interpolated value is then transferred to the reflected velocity space grid point using Equation 3. The amount of bookkeeping required to perform these calculations for a Cartesian grid is somewhat more complicated than that for a conformally mapped grid. The results of applying the specular reflection boundary condition in a two-dimensional velocity space for various incident angles are shown in Figures 5 to 7.

$$\vec{\xi}_i = \vec{\xi}_r - 2\hat{n}\left(\vec{\xi}_r \cdot \hat{n}\right) \text{ for } \vec{\xi}_r \cdot \hat{n} \geq 0 \quad (1)$$

$$f_i\left(\vec{\xi}_i\right) = \frac{1}{A}\left(A_{m,n} f_{m,n} + A_{m,n+1} f_{m,n+1} + A_{m+1,n} f_{m+1,n} + A_{m+1,n+1} f_{m+1,n+1}\right) \quad (2)$$

$$f_r\left(\vec{\xi}_r\right) = f_i\left(\vec{\xi}_i\right) \quad (3)$$

Diffuse Reflection Boundary Condition

As mentioned in the previous section, specular

reflection is not a true representation of how molecules interact with the surface. Since, on a molecular level, surfaces are not perfectly smooth, it is reasonable to assume that molecules will not reflect from a surface in a specular manner. The diffuse reflection boundary condition is a better approximation (Figure 8).

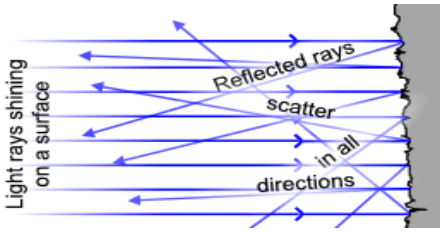

FIG. 8 DIFFUSE REFLECTION

A rough surface can be modeled by using a degree of randomization to vary the velocity of the reflected particle. One approach is to use the Maxwellian distribution to simulate diffuse reflection of the incident molecules in a quasi-equilibrium state. A more fundamental approach can be used to simulate a diffuse reflection since the relaxation phase of direct methods tends to equilibrate the mixture at a given point in physical space. A uniformly distributed set of random numbers can be used to determine the scattering direction and speed. The molecular speed values can be generated using the cumulative distribution function and uniformly distributed random numbers (Shen, 2005).

$$\left|\vec{\xi}_r\right| = \frac{1}{\beta}\sqrt{-\ln(ranf)} \quad \text{where } 0 \le ranf < 1 \tag{4}$$

$$\beta = \left(2\frac{k}{m}T_r\right)^{-1/2} \tag{5}$$

Similarly, the scattering direction can be approximated using uniformly distributed random numbers. For a two-dimensional velocity space, the scattering direction is determined from a uniformly distributed random number between zero and, as shown in Equation 6. For a three-dimensional velocity space, the scattering direction in the plane parallel to the surface also needs to be considered. Equation 7 can be used to generate this component of the scattering direction.

$$\theta = \pi \cdot ranf \quad \text{and } 0 \le ranf < 1 \tag{6}$$

$$\varphi = 2\pi \cdot ranf \quad \text{and } 0 \le ranf < 1 \tag{7}$$

The pre-collision probabilities are then distributed to the reflected velocity space grid using a weighted area distribution for a two-dimensional velocity space. A weighted volume distribution can be used for a three-dimensional velocity space. Since the reflected velocity will normally fall inside of a velocity space grid cell, but not on a specific node, the probability needs to be distributed to the neighbouring velocity space grid points. Equation 8 is used to distribute the probability to the neighbouring grid points. The cumulative probability at each velocity space grid point is determined using Equation 9. In this context, the cumulative probability refers to the sum of all the probabilities from contributing collisions to a given velocity space grid point.

$$f_{m,n} = \frac{A_{m,n}}{A} f_r\left(\vec{\xi}_r\right) \tag{8}$$

$$f_r\left(\vec{\xi}\right) = \sum_i \left(f_{m,n}\right)_i \tag{9}$$

The results of applying the diffuse reflection boundary condition in a two-dimensional velocity space for various incident angles are shown in Figures 9 to 11.

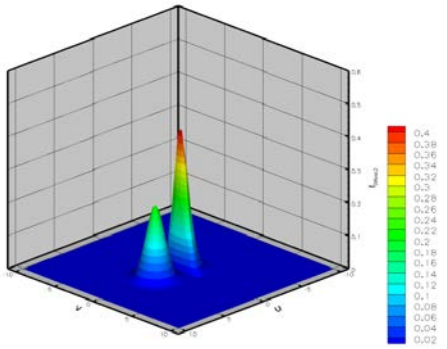

FIG. 9 DIFFUSE REFLECTION BOUNDARY CONDITION, INCIDENT ANGLE=90°

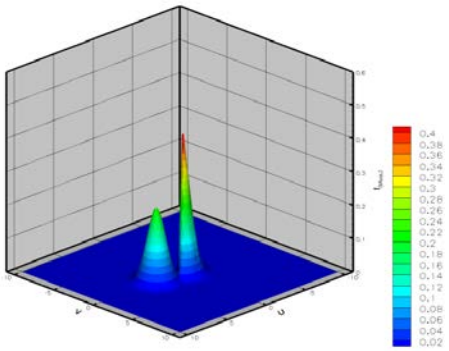

FIG. 10 DIFFUSE REFLECTION BOUNDARY CONDITION, INCIDENT ANGLE=45°

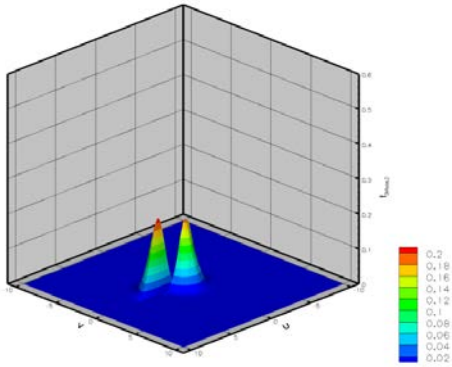

FIG. 11 DIFFUSE REFLECTION BOUNDARY CONDITION, INCIDENT ANGLE=0°

Maxwellian Reflection Boundary Condition

The Maxwellian boundary condition is a combination of specular and diffuse reflection. It is assumed that a certain percentage of incident molecules undergo specular reflection. The remaining proportion of molecules undergoes diffuse reflection. The percentage of molecules that undergo diffuse reflection is called the accommodation coefficient, α. The probability distribution is determined using Equation 10.

$$f_{Maxwellian} = \alpha f_{Diffuse} + (1-\alpha) f_{Specular} \quad (10)$$

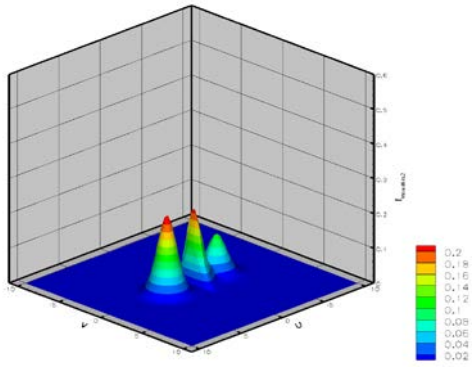

FIG. 12 MAXWELLIAN REFLECTION BOUNDARY CONDITION, INCIDENT ANGLE=90°

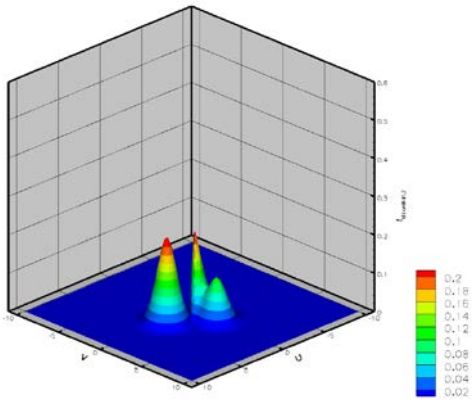

FIG. 13 MAXWELLIAN REFLECTION BOUNDARY CONDITION, INCIDENT ANGLE=45°

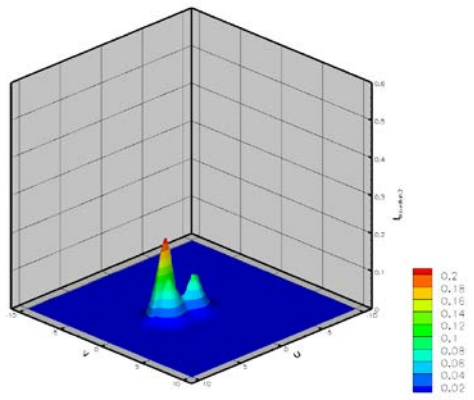

FIG. 14 MAXWELLIAN REFLECTION BOUNDARY CONDITION, INCIDENT ANGLE=0°

The accommodation coefficient, α, can be adjusted to reflect differences in the surface finishes. To a certain extent, the accommodation coefficient can be used empirically to match experimental data. Some of the factors that the accommodation coefficient could take into account include surface material, surface finish, surface porosity, surface dimensional characteristics, gas mixture constituents, and degree of rarefaction. The results of applying the Maxwellian reflection boundary condition in a two-dimensional velocity space for various incident angles are shown in Figures 12 to 14. The value of the accommodation coefficient, α, is equal to 0.5.

Adsorptive Maxwellian Reflection Boundary Condition

This last boundary condition is a combination of adsorption and Maxwellian reflection. As with the pure Maxwellian reflection, the relative proportion of molecules undergoing specular or diffuse reflections is assumed. This proportion is set using the conventional accommodation coefficient. A new coefficient, β, is introduced to represent the proportion of molecules that experience adsorption. The remaining molecules are assumed to experience the Maxwellian reflection, which is distributed between specular and diffuse reflections according to the selected accommodation coefficient. The probability distribution function is determined using Equation 11.

$$f_{Adsorptive-Maxwellian} = \beta f_{Adsorptive} + (1-\beta)\left(\alpha f_{Diffuse} + (1-\alpha) f_{Specular}\right) \quad (11)$$

The two coefficients, α and β, can be adjusted to reflect differences in surface finishes. As with the purely Maxwellian reflection, these coefficients can also be used to match experimental data. Some of the same factors addressed using the purely Maxwellian reflection can be better addressed using the adsorptive Maxwellian reflection since adsorption is included in the boundary condition. Depending on the surface properties and the constituents of the gas, a certain degree of adsorption can be expected. The adsorptive Maxwellian boundary condition allows all the three types of surface interactions to be considered. The results of applying the adsorptive Maxwellian boundary condition in a two-dimensional velocity space for various incident angles are shown in Figures 15 to 17. The selected values of the two coefficients α and β are equal to 0.5 and 0.33 respectively. As a result, the probability distribution function is composed of equal parts of adsorption, specular reflection, and

diffuse reflection.

It is clear by examining the Figures 15-17 that the probabilities associated with the specular reflection component are reduced beyond that of the Maxwellian reflection. This behaviour is expected since the specular reflection only comprises one third of the total reflection. Interestingly though, the magnitude of the diffuse reflection component located at the origin of the velocity space appears unchanged. This appearance is not accurate since the adsorptive boundary condition, which is also located at the origin of the velocity space, now comprises part of the reflected boundary condition. In other words, the contribution of the diffuse reflection is diminished by the coefficients selected for the adsorptive Maxwellian reflection. However, the part of the diminished diffuse reflection is replaced by the contribution of the adsorptive boundary condition. This behaviour continues as the angle of incidence decreases toward zero. It is important to note that the behaviour mentioned in the preceding discussion will undoubtedly change if different values for α and β are chosen.

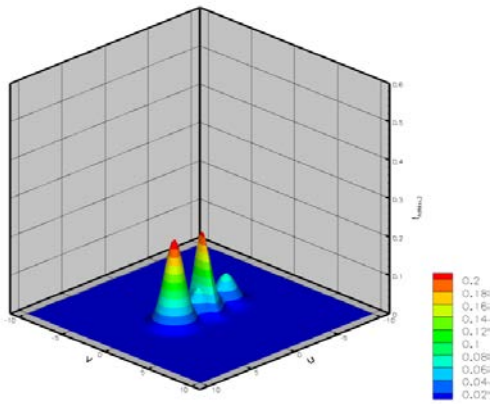

FIG. 15 ADSORPTIVE MAXWELLIAN BOUNDARY CONDITION, INCIDENT ANGLE=90°

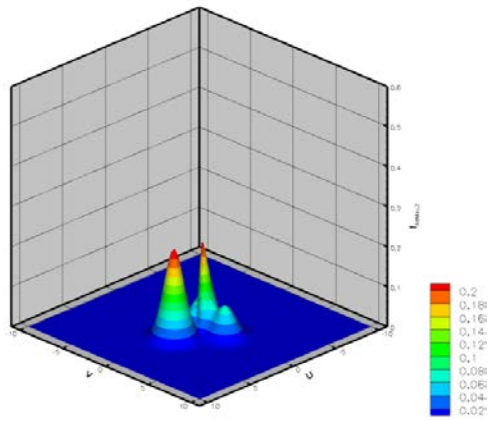

FIG. 16 ADSORPTIVE MAXWELLIAN BOUNDARY CONDITION, INCIDENT ANGLE=45°

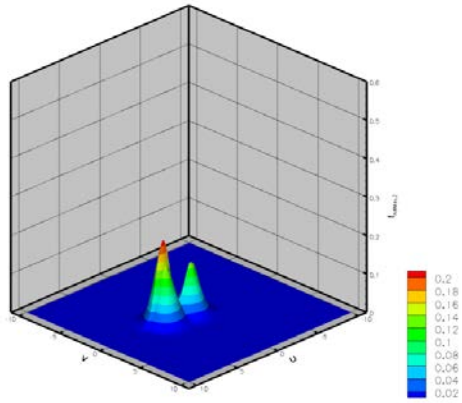

FIG. 17 ADSORPTIVE MAXWELLIAN BOUNDARY CONDITION, INCIDENT ANGLE=0°

Application of Boundary Conditions to Supersonic Flow over a Flat Plate

The solid wall boundary conditions discussed in the preceding section were applied to simulations of supersonic flow over a flat plate. These simulations were conducted in order to make a preliminary determination regarding the effectiveness of each type of boundary condition in simulating the flow near a solid wall boundary. High levels of physical space grid refinement are difficult to achieve with the existing code. Excessive memory requirements have forced the velocity space grid to be excessively coarse. The physical space grid shown in Figure 18 was used to make the preliminary assessment on solid wall boundary conditions. The cells near the surface of the flat plate have an aspect ratio equal to unity and the dimension of each side is equal to 0.1. The local Knudsen number for these cells is equal to 10, which is well into the rarefied regime. The depth of the physical space domain is equal to one mean free path.

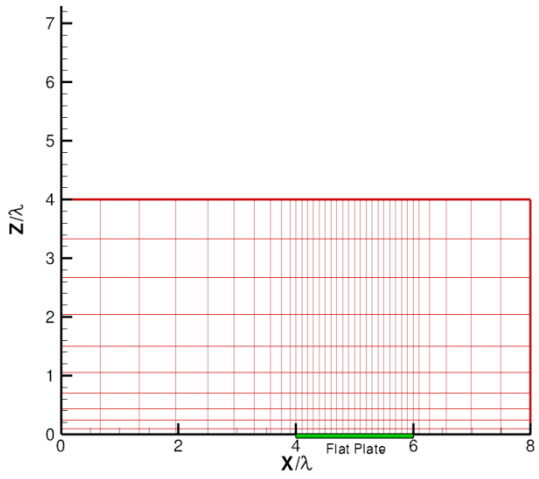

FIG. 18 FLAT PLATE GRID

The five solid wall boundary conditions discussed in

the preceding section were evaluated at a free-stream Mach number of 3.0. The equivalent Knudsen number is 0.5 since the flat plate extends between 4.0 and 6.0 in the X/λ direction in Figure 18. A wall temperature equal to the free-stream value has been assumed for the adsorptive boundary condition. The Mach number and density contours for the adsorptive boundary condition are shown in Figure 19. It can be seen from Figure 19 that the slip velocity at the wall, with the adsorptive boundary condition, is approximately equal to Mach 0.8. Additionally, a localized rise in density is experienced just upstream of the flat plate. This increase in density can be attributed to the inherent stagnation associated with the adsorptive boundary condition and the displacement of the supersonic flow by the boundary layer near the surface.

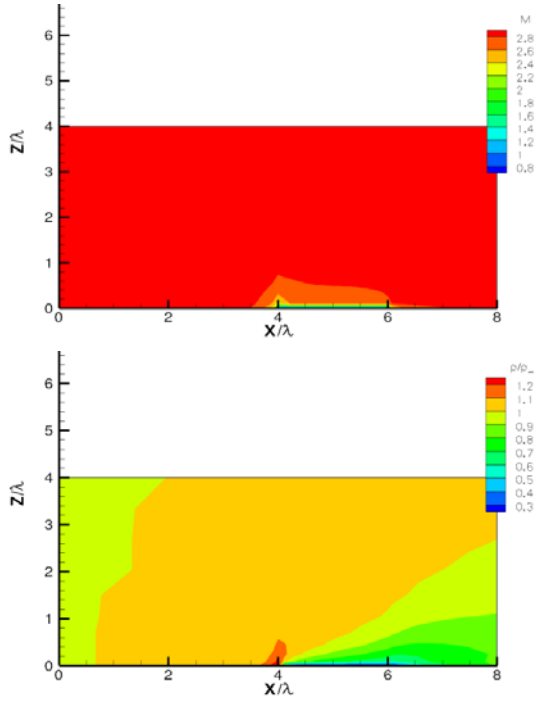

FIG. 19 FLAT PLATE MACH NUMBER AND DENSITY CONTOURS, ADSORPTION BOUNDARY CONDITION

The results obtained from the specular reflection boundary condition are unremarkable. The reflection occurs in a direction normal to the surface of the flat plate. The mean value of the distribution function around the surface normal results in a mean velocity in the Z/λ direction equal to zero. In other words, the reflection occurs about an ordinate axis in velocity space. Therefore, there is no change in the distribution function as a result of the collisions with the solid boundary. As a result, the flat plate appears as a slip line. It can be concluded that the specular reflection boundary condition corresponds to an inviscid boundary in a continuum solver. The Mach number and density contours for the specular reflection boundary condition are shown in Figure 20.

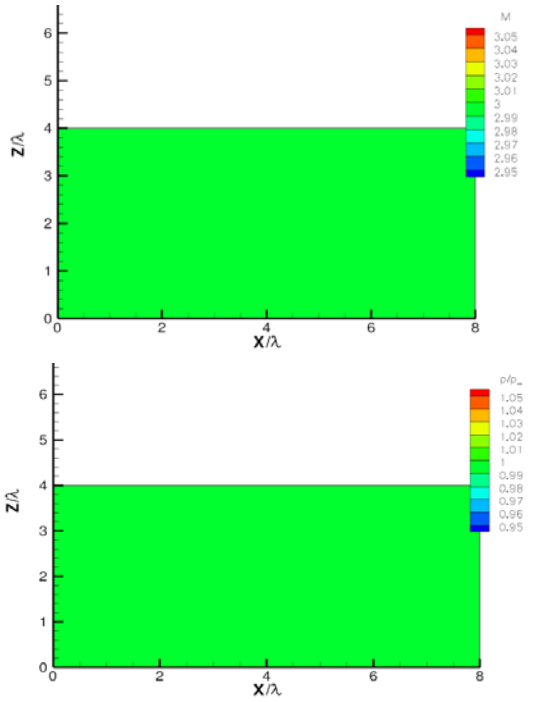

FIG. 20 FLAT PLATE MACH NUMBER AND DENSITY CONTOURS, SPECULAR REFLECTION BOUNDARY CONDITION

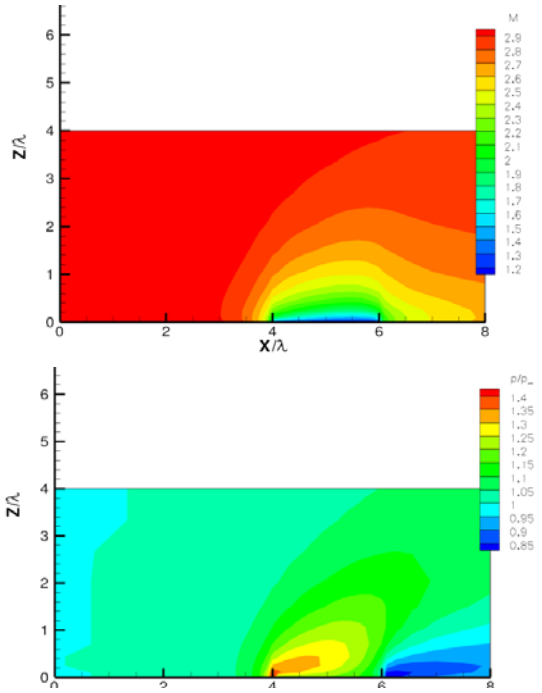

FIG. 21 FLAT PLATE MACH NUMBER AND DENSITY CONTOURS, DIFFUSE REFLECTION BOUNDARY CONDITION

The Mach number and density contours for the diffuse reflection boundary condition are presented in Figure 21. The slip velocity for the diffuse reflection is approximately 1.2, as compared to 0.8 with pure adsorption. Additionally, the extent and strength of the shock wave upstream of the flat plate is more

pronounced. Similarly, the expansion fan behind the flat plate is more noticeable.

The next boundary condition implemented is the Maxwellian reflection. The Mach number and density contours are shown in Figure 22. The accommodation coefficient used for the simulation is equal to 0.5 corresponding to a distribution function at the wall composed of half specular reflection and half diffuse reflection. The strength of the shock upstream of the flat plate has been reduced. However, the diffusion of the upstream shock and the downstream expansion fan still exists. As expected, the slip velocity from the value obtained using the diffuse reflection boundary condition is approximately 2.0. A preliminary conclusion can be drawn that a linear transition between purely specular reflection and purely diffuse reflection does not result in a linear change in the flow field parameters.

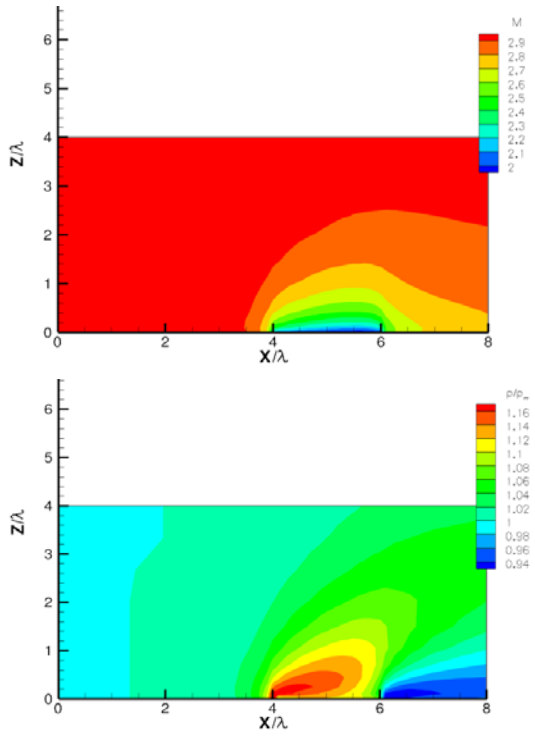

FIG. 22 FLAT PLATE MACH NUMBER AND DENSITY CONTOURS, MAXWELLIAN REFLECTION BOUNDARY CONDITION

The final boundary condition examined is the combination of adsorption and Maxwellian reflection. In this case, adsorption and Maxwellian reflection were assumed to comprise 33% and 67% of the solid wall interaction, respectively. This split results in a solid wall boundary condition composed of one third adsorption, one third specular reflection, and one-third diffuse reflection. The Mach number and density contours are shown in Figure 23. The slip velocity for the adsorptive Maxwellian boundary condition is approximately 1.3. The magnitude of the shock upstream of the flat plate is lower than that obtained from the Maxwellian reflection. Additionally, the definition of the expansion fan downstream of the flat plate is reduced, which corresponds to the decrease in strength of the shock upstream. It is clear from Figure 23 that adsorption is the dominant phenomenon with the proportions assumed for this simulation. In other words, a little adsorption goes a long way.

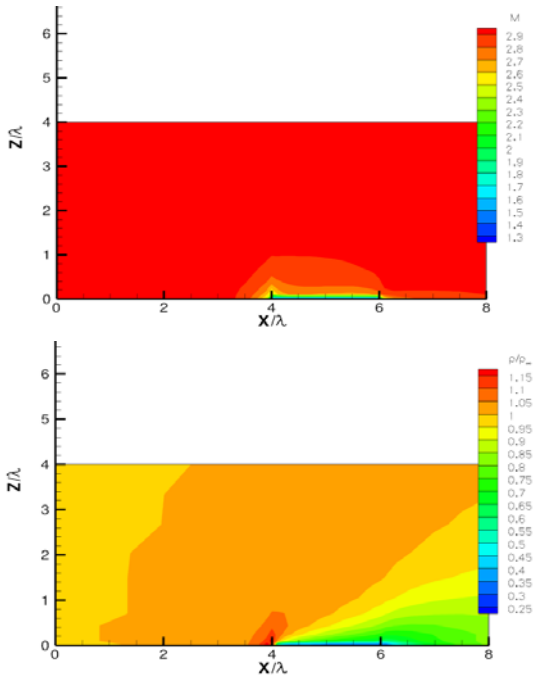

FIG. 23 FLAT PLATE MACH NUMBER AND DENSITY CONTOURS, ADSORPTIVE MAXWELLIAN REFLECTION BOUNDARY CONDITION

The five boundary conditions can also be compared by calculating the partial derivatives that are proportional to skin friction and heat transfer. These derivatives are presented in Equations 12 and 13.

$$q \propto \frac{\partial(T/T_\infty)}{\partial(Z/\lambda)} \tag{12}$$

$$c_f \propto \frac{\partial(U/U_\infty)}{\partial(Z/\lambda)} \tag{13}$$

A comparison of these derivatives can assist in understanding the relationship among each of the various solid wall boundary conditions presented in this paper. Figure 24 presents a comparison of the heat transfer properties and skin friction along the surface of the flat plate. Both sets of data are compared with the continuum boundary layer approximation given in Schlichting (1968).

As expected, the heat transfer and skin friction for the specular reflection boundary condition is zero across the entire surface of the flat plate. The diffuse reflection boundary condition results in heat transfer

values that are not too dissimilar from the specular reflection values. However, the skin friction values are higher for diffuse reflection. When combining specular and diffuse reflection, in the form of Maxwellian reflection, the skin friction falls between the values obtained for specular reflection and the diffuse reflection. Interestingly, the Maxwellian reflection results in absolute values of heat transfer higher than those obtained from either specular reflection or diffuse reflection. The adsorptive boundary condition yields the highest skin friction values and the highest absolute heat transfer values. When combined with the Maxwellian reflection, the adsorptive boundary condition dominates the heat transfer process and results in a profile that is almost the same as pure adsorption, as well the skin friction values, but to a lesser extent.

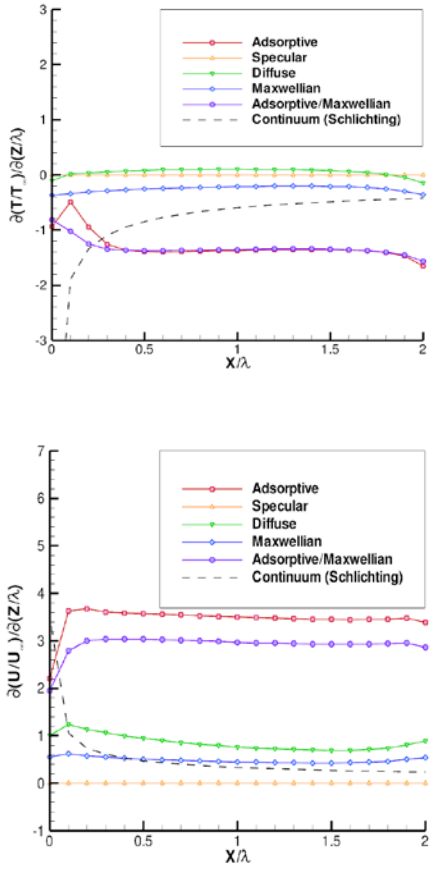

FIG. 24 HEAT TRANSFER AND SKIN FRICTION ON A FLAT PLATE USING FIVE DIFFERENT BOUNDARY CONDITIONS, M=3

Conclusions

For numerical solution of the Generalized Boltzmann equation for rarefied flow past solid bodies, five different solid wall boundary conditions– adsorptive, specular, diffuse, Maxwellian and adsorptive Maxwellian are considered. These boundary conditions are evaluated by computing the supersonic flow past a flat plate. For supersonic flow over a flat plate, pure adsorption results in the highest values of skin friction and heat transfer. Pure specular reflection causes the lowest values of skin friction and heat transfer. Diffuse reflection results in skin friction values that fall between the adsorptive and specular reflection values. The Maxwellian reflection yields some flexibility in tuning the skin friction and heat transfer values across the plate. However, combining the adsorptive boundary condition with the Maxwellian reflection enables an even greater degree of flexibility. This flexibility will be very useful when attempting to match the numerical simulations to experimental data.

REFERENCES

Agarwal, R. K. and Tcheremissine, F.G., "Computation of Hypersonic Shock Wave Flows of Diatomic Gases and Gas Mixtures Using the Generalized Boltzmann Equation," AIAA Paper 2010-813, 48th AIAA Aerospace Sciences Meeting Including the New Horizons Forum and Aerospace Exposition, Orlando, Florida, 4-7 January 2010.

Qian, G., Agarwal, R.K., and Wilson, C.D.," Computations of Shock Waves in Inert Binary Mixtures in Non-Equilibrium Using Generalized Boltzmann Equation," Frontiers of Aerospace Engineering, 2(2013):1-12.

Qian, G., Agarwal, R.K., and Wang, B., Computation of Hypersonic Flow past a Blunt Body in an Inert Binary Gas Mixture in Rotational Non-equilibrium Using the Generalized Boltzmann Equation," Frontiers of Aerospace Engineering, Vol.2, Issue 3, September 2013.

Schlichting, H., Boundary Layer Theory, New York: McGraw-Hill, 1968.

Shen, C., Rarefied Gas Dynamics: Fundamentals, Simulations & Micro Flows, Berlin: Springer-Verlag, 2005.

Tcheremissine, F.G., "Solution of the Wang-Chang-Uhlenbeck Master Equation," Doklady Physics, 47 (2002): 872-875.

Wilson, C. D., Agarwal, R. K. and Tcheremissine, F. G., "Computation of Hypersonic Shock Waves in Inert Gas Mixtures Using the Generalized Boltzmann Equation," AIAA Paper 2011-3134, AIAA 42nd Thermophysics Conference, Hawaii, 27-30 June 2011.